Calhoun

Institutional Archive of the Naval Postgraduate School

Calhoun: The NPS Institutional Archive

2007

Secondary eyewall formation in two idealized, full-physics modeled hurricanes

Terwey, W. D.

Secondary eyewall formation in two idealized, full-physics modeled hurricanes

Wesley D. Terwey[1,4] and Michael T. Montgomery[2,3]

[1] Prevailing hypotheses for secondary eyewall formation are examined using data sets from two high-resolution mesoscale numerical model simulations of the long-time evolution of an idealized hurricane vortex in a quiescent tropical environment with constant background rotation. The modeled hurricanes each undergo a secondary eyewall cycle, casting doubt on a number of other authors' hypotheses for secondary eyewall formation due to idealizations present in the simulation formulations. A new hypothesis for secondary eyewall formation is proposed here and is shown to be supported by these high-resolution numerical simulations. The hypothesis requires the existence of a region with moderate horizontal strain deformation and a sufficient low-level radial potential vorticity gradient associated with the primary swirling flow, moist convective potential, and a wind-moisture feedback process at the air-sea interface to form the secondary eyewall. The crux of the formation process is the generation of a finite-amplitude lower-tropospheric cyclonic jet outside the primary eyewall with a jet width on the order of a local effective beta scale determined by the mean low-level radial potential vorticity gradient and the root-mean square eddy velocity. This jet is hypothesized to be generated by the anisotropic upscale cascade and axisymmetrization of convectively generated vorticity anomalies through horizontal shear turbulence and sheared vortex Rossby waves as well as by the convergence of system-scale cyclonic vorticity by the low-level radial inflow associated with the increased convection. Possible application to the problem of forecasting secondary eyewall events is briefly considered.

1. Introduction

[2] Secondary eyewalls (also known as concentric eyewalls) are perhaps one of the more enigmatic features of fully developed tropical cyclones and hurricanes. Once regarded as an infrequent occurrence during a tropical cyclone's lifecycle, studies of this phenomenon using aircraft reconnaissance radar data and high-resolution microwave satellite data have shown that upwards of 50% of all major tropical cyclones undergo at least one eyewall replacement cycle in their lifetimes [*Willoughby et al.*, 1982; *Hawkins and Helveston*, 2004], making this a well-known forecasting issue in major tropical cyclones.

[3] Observations of secondary eyewall cycles gathered during the last three decades [*Willoughby et al.*, 1982; *Black and Willoughby*, 1992; *Willoughby and Black*, 1996; *Houze et al.*, 2007] and theoretical dynamics [e.g., *Shapiro and Willoughby*, 1982] have suggested that the effects of the secondary eyewall phenomenon on the intensity of a storm can be significant, particularly in the short-term.

[4] An illustrative example is Hurricane Ivan (2004) in the Atlantic Ocean, as seen in Figure 1. Ivan entered the Caribbean Sea on 8 September 2004 as a major hurricane. As Ivan approached the island of Jamaica, a secondary eyewall formed, as seen in aircraft radar data from near Jamaica (Figure 1b). As the secondary eyewall matured, the minimum central pressure (Figure 1a) rose 15 mb in approximately 18 h. According to aircraft reconnaissance data, the reported wind speed of Ivan also dropped 10 to 15 knots during this time period, a substantial intensity decrease from the maximum of 140 knots prior to the secondary eyewall cycle (not shown). While there was likely some influence on the strength of Ivan's outer circulation by the Jamaican landmass, the inner-core region (composed of the eye and primary eyewall) of the storm was far enough from the island (approximately 200–600 km through the secondary eyewall cycle) to support the hypothesis that the secondary eyewall was the dominant influence on the observed short-term intensity fluctuation [e.g. *Willoughby et al.*, 1982, 1985].

[5] In the past, the primary theoretical focus has been directed at the evolution of the secondary eyewall and its interaction with the primary eyewall [*Willoughby et al.*,

[1]Department of Atmospheric Science, Colorado State University, Fort Collins, Colorado, USA.
[2]Department of Meteorology, Naval Postgraduate School, Monterey, California, USA.
[3]NOAA, Hurricane Research Division, Miami, Florida, USA.
[4]Department of Earth Sciences, University of South Alabama, Mobile, Alabama, USA.
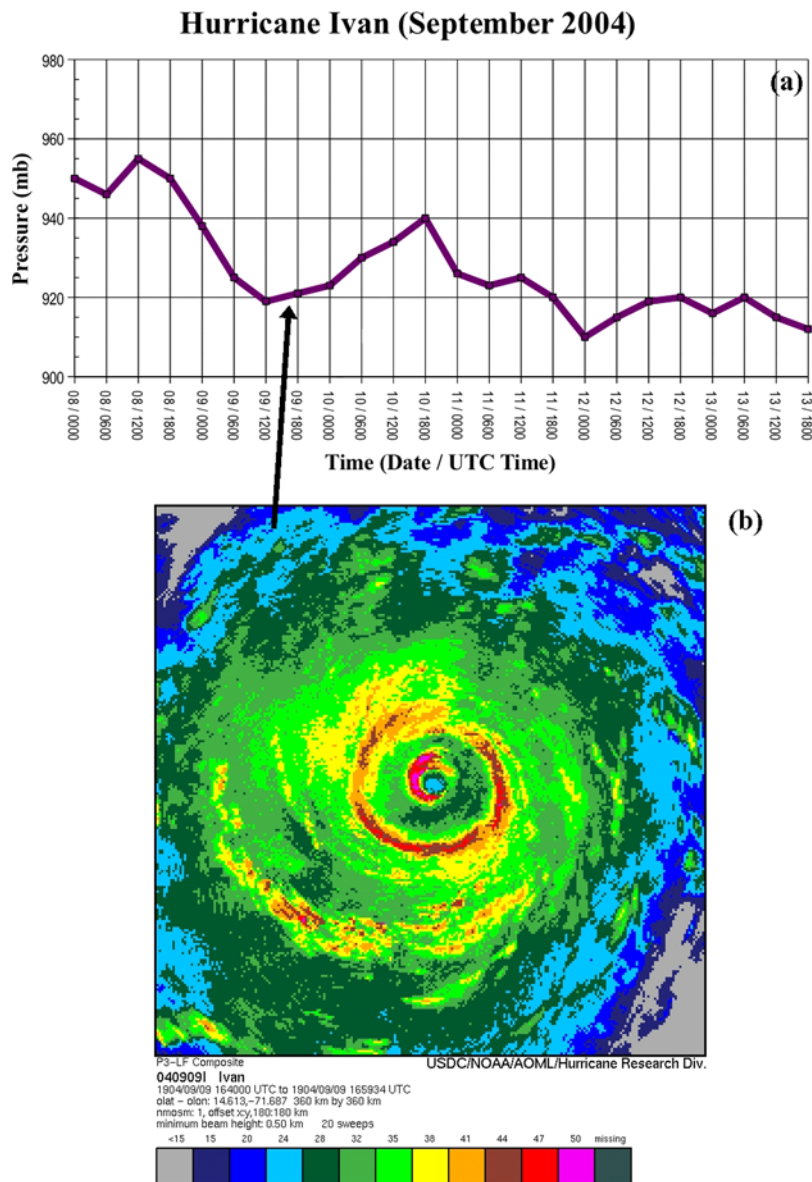
Figure 1. (a) Best track sea-surface pressure trace from the National Hurricane Center for Hurricane Ivan (2004). (b) Research aircraft radar reflectivity composite of Ivan with two eyewalls. At this time, the central pressure is about to begin increasing, indicating a temporary decrease in the intensity of the storm correlated with the secondary eyewall cycle. Kingston, Jamaica is approximately 600 km northwest of the storm center at this time. Figure 1b is courtesy of the NOAA Hurricane Research Division of AOML.

1982; *Shapiro and Willoughby*, 1982]. In these theories, the transverse circulation associated with the secondary eyewall forces a gradual spindown of the strong tangential winds near the primary eyewall by inducing a weakly divergent radial wind field there. Additionally, this circulation forces subsidence in the region surrounding the primary eyewall, inhibiting its convection. As these processes temper the winds and convection associated with the original eyewall, the secondary eyewall strengthens and assumes the role of the primary eyewall of the cyclone. The combined changes associated with the strengthening secondary eyewall and the weakening primary eyewall generally decrease the magnitude of the maximum mean tangential winds of the system and increase the minimum surface pressure [e.g., *Willoughby et al.*, 1985]. After this occurs, the new eyewall typically

contracts, reconsolidating the swirling winds of the storm toward the center.

[6] The eyewall evolution theory has proven qualitatively useful in describing intensity changes in mature hurricanes due to eyewall cycles [e.g., *Willoughby et al.*, 1984; *Willoughby and Black*, 1996; *Houze et al.*, 2006, 2007]. One of the challenges still facing hurricane forecasters, however, is that a secondary eyewall cycle may happen multiple times through the lifetime of long-lived mature tropical cyclones, or it may never occur. The mechanisms that determine whether or not a secondary eyewall cycle occurs in a given hurricane are as of yet unknown, and much of the unknown appears to exist in the weakness of the cycle theory: the processes that cause the formation of the secondary eyewall in the first place.

[7] During the past three decades, a number of hypotheses have been proposed to describe the formation of the secondary eyewall. *Willoughby et al.* [1982], borrowing ideas developed for tropical squall lines by *Zipser* [1977], suggested that downdrafts from the primary eyewall's convection might force a ring of updrafts outside of it. *Hawkins* [1983] proposed that topographic effects might form a secondary eyewall. Other results [*Molinari and Skubis*, 1985; *Molinari and Vallaro*, 1989] have suggested that large-scale environmental forcings, such as inflow surges or upper-level angular momentum fluxes from intruding potential vorticity anomalies, may be causes of general eyewall formation. *Willoughby* [1979] hypothesized the existence of an internal resonance between the local inertia period and asymmetric friction due to the storm's motion could form a new eyewall. Additionally, ice microphysics has been suggested as an enhancement mechanism in secondary eyewall formation [*Willoughby et al.*, 1984].

[8] More recently, simple numerical modeling experiments have been used to investigate the secondary eyewall formation process. Using axisymmetric hurricane models developed by *Emanuel* [1989, 1995] and *Rotunno and Emanuel* [1987], *Nong and Emanuel* [2003] carried out a number of idealized simulations and concluded that sustained eddy angular momentum fluxes arising from interactions between a mature storm and its synoptic environment can form secondary eyewall features, provided a surface-wind/water vapor feedback operates in the same region. This wind-induced surface heat exchange process is now commonly known as WISHE [*Yano and Emanuel*, 1991]. From the perspective of barotropic nondivergent vorticity dynamics, *Kuo et al.* [2004, 2008] suggested that secondary eyewall formation arises essentially from the axisymmetrization of cyclonic vorticity perturbations around a strong primary vortex core.

[9] It has not been until very recently, however, that three-dimensional full-physics numerical models have shown the ability to simulate a secondary eyewall cycle. In the current work we examine a pair of idealized long-time hurricane simulations using a full-physics three-dimensional mesoscale model. These simulations are shown to produce realistic tropical cyclones, including a complete secondary eyewall cycle, under both full (ice and water) and water-only moist physical representations. Using the model data sets generated by the simulations, we analyze the basic physics of secondary eyewall initiation, testing and drawing ideas from previous hypotheses for this complex process. Prior formation hypotheses are summarized and many are rejected as necessary criteria for our particular cases, generally because of the specific idealizations assumed by the model setup. A new hypothesis along with supporting evidence is presented here for an intrinsic secondary eyewall formation mechanism that involves a turbulent, horizontally anisotropic, upscale energy cascade of convectively generated small-scale eddies in an anticyclonic shear zone outside the main core of the hurricane. While the axisymmetrization ideas of numerous previous works [e.g., *Melander et al.*, 1987; *Montgomery and Kallenbach*, 1997; *Kuo et al.*, 2004, 2008] lay a useful foundation for the problem, our hypothesis extends these ideas to account for the sustained potential vorticity injection via cumulus convection and

related convective scale phenomenology that occur within the hurricane.

[10] In studying these idealized and simplified cases of secondary eyewall formation, we seek to find the most basic theory to describe the phenomenon. From this point, additional work can be pursued to identify the strengths and weaknesses of the proposed theory and to develop a more complete understanding of the pertinent multiscale fluid dynamical and thermodynamical interactions. We furthermore anticipate that this theory forms a foundation for the forecasting of secondary eyewall cycles in real tropical cyclones, as well as providing a framework for understanding how other complications present in real tropical cyclones (shear, environmental interactions, oceanic upwelling) may or may not fit into the theory.

[11] Section 2 describes the model setup, including the initial conditions and the simplifications used. Section 3 summarizes the evolution of the control hurricane simulation that spontaneously generates a secondary eyewall. Previous secondary eyewall formation hypotheses are then assessed in section 4 with regard to the control simulation, and a new formation paradigm is proposed. Section 5 focuses on the pertinent dynamical diagnostics and theories used to offer supporting evidence for the hypothesized formation mechanism. A summary of the water-only microphysical species sensitivity experiment is presented in section 6. This "reduced physics" experiment also produces a secondary eyewall cycle, and we briefly show the similarity of the results between these two experiments. Last, in section 7, we summarize our findings and discuss future planned work for these and related numerical experiments, as well as for the examination of our findings in observational data sets.

2. Model Details

2.1. RAMS Model

[12] For this study, we employ the Regional Atmospheric Modeling System (RAMS) [*Pielke et al.*, 1992; *Cotton et al.*, 2003]. The RAMS is a three-dimensional, nonhydrostatic numerical modeling system with equations for the time-dependent changes of velocity, nondimensional pressure perturbation, ice-liquid water potential temperature [*Tripoli and Cotton*, 1981], and cloud microphysics including seven moist particulate species. Diagnostic equations include those for potential temperature and vapor mixing ratio [*Tripoli and Cotton*, 1982].

[13] The microphysical scheme includes seven species: cloud droplets, rain, pristine ice, snow, aggregates, graupel, and hail. The microphysical scheme can be run in one or two-moment modes and was developed by *Walko et al.* [1995]. In our simulations, we exclusively utilize the simpler one-moment schemes with the exception of pristine ice [*Montgomery et al.*, 2006, Appendix A]. We have run two simulations for this work. The first uses all seven microphysical species. The second only includes the cloud droplet and rain species. We call this latter sensitivity simulation the "no ice" simulation while the former is called the "control" simulation.

[14] Surface flux parameterizations for latent heat, sensible heat and momentum are based on the *Louis* [1979] scheme. The radiation scheme for both long wave and short

wave radiation developed by *Harrington* [1997] is used, which includes cloud microphysical interactions. The subgrid scale turbulence scheme used is based on *Smagorinsky* [1963] with modifications from *Lilly* [1962] and *Hill* [1974]. These modifications enhance diffusion in unstable conditions while reducing diffusion in stable conditions.

[15] Multiple nested grids are used in the simulations, developed from the work of *Clark and Farley* [1984]. The grids are two-way interactive, allowing for increased spatial resolution in areas where one desires explicit representation of cloud scale features.

2.2. Experimental Design

[16] To simulate a hurricane vortex through a long period of its life, the simulation domain is made sufficiently large to ensure that the storm dynamics are not influenced by the outer boundary conditions. Three nested grids are therefore used with uniform horizontal grid spacing of 24, 6, and 2 km and 168, 170, and 251 grid points on each grid, respectively. This translates to respective horizontal grid domain lengths of 4032, 1020, and 502 km. Each inner grid is centered on the center of the outermost grid. To help ensure that the simulated storm remains near the center of the domain, we initialize the environment to be at rest (excluding the weak mesoscale convective vortex at the center). Additionally, we run the model on an f-plane centered at 15°N; this neglects the meridional gradient of planetary vorticity that induces a northwestward vortex motion [e.g., *McWilliams and Flierl*, 1979; *Shapiro*, 1992]. The f-plane configuration guarantees that the bulk of the convective-scale dynamics are represented on the 2 km grid.

[17] The outermost grid is made cyclic in the horizontal directions to help ensure that mass and wind remain continuous in the domain. Given that the typical hurricane vortex comprises an area that is a small fraction of the approximately 16,000,000 km^2 outer grid, it is believed that the cyclic boundary condition coupled with the large domain size should be sufficient to prevent the simulated storm from interacting strongly with itself.

[18] The model has 30 vertical levels stretching nonuniformly from the surface to approximately 26 km in height. The vertical grid spacing starts at 300 m near the surface and increases to 1800 m at the top of the domain, utilizing a stretch factor of 1.065. We use a rigid bottom boundary with latent and sensible heat fluxes most appropriate to represent a flat sea surface. The sea surface temperature is fixed throughout all domains at 28°C. The upper boundary is closed, but includes a Rayleigh "sponge" layer exclusively in the stratosphere (uppermost six levels) to strongly damp upward propagating gravity waves and artificial gravity wave reflection off the model top.

[19] The model's initial condition is similar to the initial vortex used by *Montgomery et al.* [2006, hereafter referred to as M06]. As in M06, the control simulation was initialized with a mesoscale convective vortex (MCV) in gradient and hydrostatic balance with radius of maximum winds (RMW) at 75 km from the center of circulation and 4 km altitude above the sea surface, quantitatively similar to observations [e.g., *Bister and Emanuel*, 1997; *Raymond et al.*, 1998; *Reasor et al.*, 2005]. The maximum tangential wind speed of the initial MCV in the M06 control simula-

tion is approximately 6.5 m s^{-1}. Because of the large computational and data storage demands required to carry out these extended tropical cyclone lifecycle experiments, the initial wind speed maximum of the MCV is increased to approximately 10 m s^{-1} so as to generate a tropical storm surface vortex somewhat sooner than the M06 control experiment. Convection is stimulated with a warm bubble near the RMW at the start of the simulation. The initial vertical sounding is based off the *Jordan* [1958] climatological hurricane season sounding as described in M06. Outside the MCV, the environment is initialized with this basic sounding. Near the center of the initial MCV, though, the lower and middle layers of the sounding are moistened somewhat to account for increased sea-to-air moisture fluxes in the vicinity of the vortex. The moistening anomaly results in an increase in the water vapor mixing ratio by 1.3 g kg^{-1} near the surface in the center of the MCV.

[20] Two temporal views of the simulated control storm are summarized here. The first is the complete 204-h simulation at three-hour output intervals, giving an overview of the entire simulated evolution. The second view begins at 156 h, running for 24 h with a 6-min output interval.

3. Vortex Evolution Summary

[21] Figure 2 shows the evolution of the storm utilizing three commonly used hurricane metrics: minimum pressure, maximum azimuthal mean tangential winds, and the radius of maximum mean tangential winds (RMW). In our case, we calculate these storm metrics from the lowest model level above the surface (approximately 150 m), except for the maximum mean tangential winds, which are typically found just above the 1 km level.

[22] The model storm takes approximately 48 h to undergo the transition from a weak MCV to a hurricane-strength vortex, nearly 12 to 18 h faster than the control case in M06. After attaining tropical storm strength, the storm continues intensifying rapidly into a small hurricane vortex, as evidenced by its 10 km RMW and 40 to 50 m s^{-1} mean tangential winds.

[23] After 60 h, the storm begins a phase of intensity fluctuations that lasts for nearly 60 h. During this period, it is noteworthy that the RMW gradually increases from approximately 10 to 25 km while the maximum mean tangential winds waver around 60 m s^{-1}. The spatial expansion of a maturing hurricane vortex is not anticipated from simple theoretical considerations using axisymmetric balanced dynamics, which forecasts that slowly evolving hurricane eyewalls contract, not expand [*Shapiro and Willoughby*, 1982]. This period of expansion in the numerical simulation does not include any secondary eyewall cycles. Further analysis of this phenomenon is deferred to future research in due course.

[24] After 110 h, the storm begins intensifying once again. The maximum mean winds increase from approximately 60 m s^{-1} to over 80 m s^{-1} through the next 60 h, while the near-surface minimum pressure drops another 50 mb. At 156 h into the simulation, we denote a new time coordinate corresponding to our focused interest in this time period. We call this point in time Hour 0.

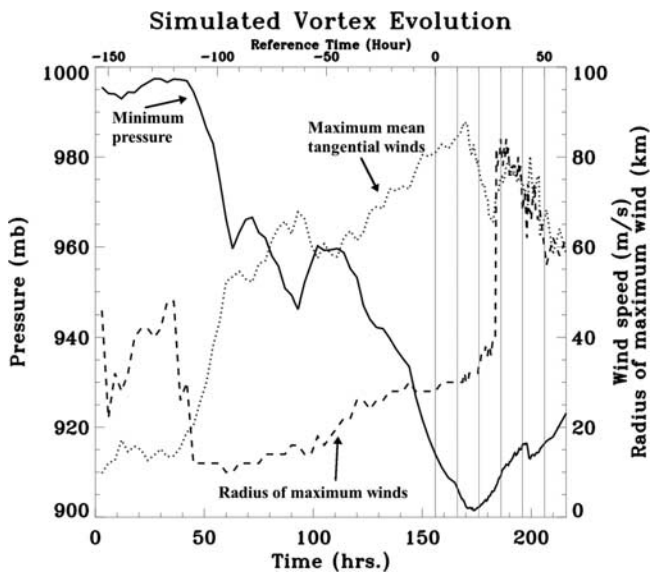[25] The storm reaches its peak intensity around Hour 16 with maximum mean tangential winds just over 85 m s^{-1}.

Figure 2. Modeled storm evolution through the simulation time for the control experiment. The solid line is the minimum pressure at 150 m above the surface. The dashed line is the radius of maximum mean tangential winds at 150 m above the surface. The dotted line is the maximum azimuthally averaged tangential winds through the domain.

After this point, Figure 2 indicates that a secondary eyewall cycle may be occurring. The maximum winds decrease rapidly (approximately 10 m s^{-1} in 6 h) while the pressure rises nearly as rapidly as it had dropped in the previous days (approximately 1 mb h^{-1}). Finally, around Hour 27, a sudden increase in the RMW from approximately 35 km to 80 km is observed. Observations suggest this is the key signature of a hurricane's reorganization after the secondary eyewall supplants the inner eyewall as the dominant eyewall in the vortex [*Willoughby et al.*, 1982; *Willoughby and Black*, 1996; *Houze et al.*, 2007].

[26] To support our assertion that this represents the beginning of a secondary eyewall cycle, we present a time-radius plot of the mean vertical velocity in the mid-levels in Figure 3. From this figure, we see the primary eyewall located between 30 and 40 km radius at Hour 0, along with some sporadic bursts of convection outside the primary eyewall. Around Hours 5 to 7, there appears to be a failed secondary eyewall formation near 70 km radius. We will not discuss this feature in this work, other than to speculate that secondary eyewall-like formations may occur more frequently than current observational data networks, such as polar orbiting microwave satellites or aircraft reconnaissance, can sample them. Another secondary eyewall formation begins taking place around Hour 16. The diffuse nature of the vertical velocities after Hour 16 in the secondary eyewall is primarily due to its strongly asymmetric nature. We hereafter refer to the region from 60 to 150 km in radius as the "formation region" and Hours 8 to 18 as the "formation period."

[27] To gain further understanding into the dynamics of the secondary eyewall initiation, we summarize the temporal changes of the convection associated with the hurricane in Figure 4, which shows horizontal cross-sections of the

vertical velocity just above 2 km height at 3-h intervals from Hour 12 to Hour 27. At Hours 12 to 15, we see a nearly circular eyewall with multiple spiral band-like convective features that spiral cyclonically inward toward the primary eyewall. The bands appear to consolidate slowly into a complete circle around the primary eyewall during Hours 18 to 21, completing the secondary eyewall between Hours 24 and 27.

[28] This secondary eyewall is generally elliptical in shape, with an eccentricity of approximately 0.65 to 0.85 through its formation and mature phases; this helps explain the diffuse nature of the mean vertical velocities displayed in the previous time-radius plot of mean vertical velocities (Figure 3). Elliptical secondary eyewalls may not be uncommon in major tropical cyclones. As an illustration, Figure 5 shows an elliptical secondary eyewall observed in Hurricane Ivan (2004). *Dodge et al.* [1999] also showed that Hurricane Gilbert (1988) had an elliptical secondary eyewall. We believe that the ovoid shape of the secondary eyewall may be part of its natural variability.

[29] After the formation period, convection associated with the inner eyewall weakens appreciably, disappearing completely by Hour 36 (not shown). The new single eyewall begins contracting slowly while axisymmetrizing. At the end of the model simulation, the storm begins a period of reorganization when a strong outer rainband forms, advecting the center toward the northern portion of the inner grid (not shown). This marks the first time in the storm's lifetime that its center has moved farther than 60 km from the model domain center.

4. Secondary Eyewall Dynamics Fundamentals

4.1. Prior Formation Hypotheses

[30] In the introduction, previous hypotheses on the formation of secondary eyewalls were briefly summarized. Using the data sets for our two numerical hurricane experiments, we now more thoroughly examine these prior
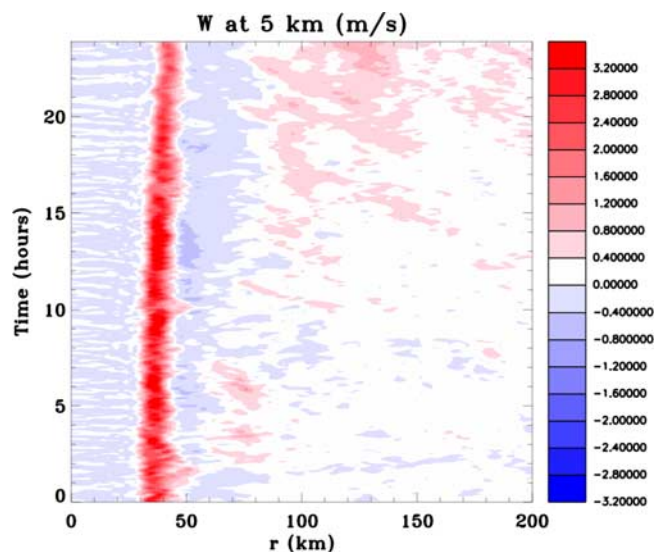

Figure 3. Time-radius plot of mean vertical velocity (m s^{-1}) at 5 km height from Hours 0 to 24 for the control experiment.
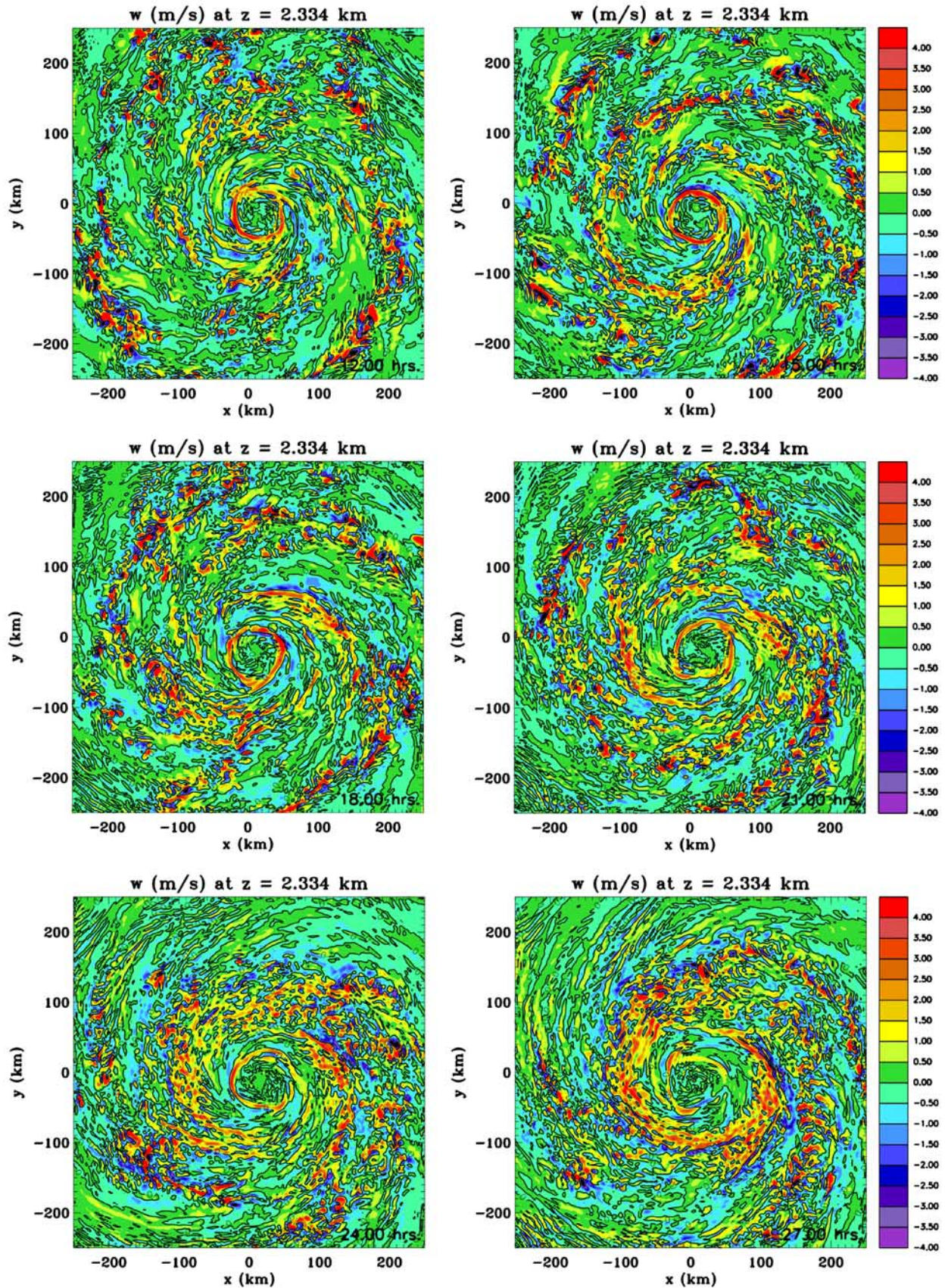
Figure 4. Vertical velocity (m s^{-1}) at the 2.33 km level for six times during the secondary eyewall formation time for the control experiment. Plots are Hour 12 (top left), Hour 15 (top right), Hour 18 (center left), Hour 21 (center right), Hour 24 (bottom left), and Hour 27 (bottom right).
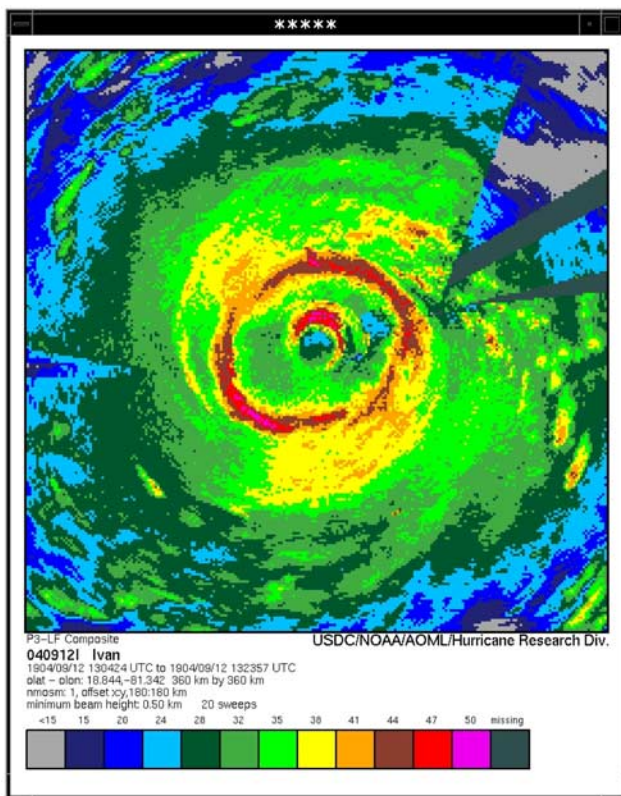
Figure 5. Composite radar reflectivity from aircraft reconnaissance into Hurricane Ivan (2004) on 12 September. Two eyewalls, including an elliptical secondary eyewall, is evident.

hypotheses, focusing on those ideas that we may be able to use to explain the secondary eyewall formations that happen in the current simulations.

[31] Table 1 summarizes the prevailing published hypotheses for secondary eyewall formation and gives a short description as to the relevance of the hypothesis with respect to our modeled storms. A number of the hypotheses are easily dismissed as unnecessary for the formation of the secondary eyewall in our simulations. *Hawkins* [1983], for example, speculated that secondary eyewalls might form due to topographic influences on the vortex circulation. However, since our simulations include no topography, topography is not required for secondary eyewall formation.

[32] Furthermore, note that the hypothesized resonance of *Willoughby* [1979] between the local inertia period and asymmetric friction due to storm motion is not a requirement for secondary eyewall formation. Neither of the simulated storms drifts more than 60 km from the center of the model domain until well after the secondary eyewall cycle has completed.

[33] The two Molinari conjectures [*Molinari and Skubis*, 1985; *Molinari and Vallaro*, 1989], and to a lesser extent the *Nong and Emanuel* [2003] conjecture, arguing for the importance of synoptic-scale influences on eyewall formation are also not necessary conditions in our simulations. We do not specify any synoptic-scale forcings in the simulation, nor do we find evidence that any form in the environment of the modeled hurricane during the simulation.

[34] The simulations presented here have been purposely formulated to omit many of these previously conjectured processes. The simulations suggest intrinsic processes operating within the hurricane act to form secondary eyewalls without processes assumed in the excluded hypotheses in Table 1. We cannot reject the possibility, however, that these previous ideas may have relevance in specific cases. Instead, we now focus our attention on the hypothesized intrinsic mechanisms for secondary eyewall formation.

[35] Regarding the *Willoughby et al.* [1982] downdraft conjecture, we note that there are gentle downdrafts on the order of 25 to 50 cm s^{-1} in the azimuthal mean and 2 to 4 m s^{-1} locally outside the core of the storm, mainly found in the middle levels of the storm. While there does appear to be some evidence that a small number of simulated updrafts are forced by previous downdrafts, these are in the minority of the updrafts diagnosed in the formation region and period (not shown). Given the lack of sufficient evidence supporting the downdraft conjecture, we hereafter reject it in our model-based examinations of secondary eyewall formation.

[36] Kuo et al. studied the two-dimensional, nondivergent vortex dynamic interactions between two or more vorticity patches of varying sizes, separations, and intensities [*Kuo et al.*, 2004, 2008]. These works have shown that concentric vorticity features will be formed by the axisymmetrization of weaker patches of vorticity around a strong core of vorticity, usually with the requirement that the weaker patches be suitably far from the core and with vorticity amplitudes at least four to six times less intense than the core vorticity. Their numerous numerical experiments highlight the robustness of this result. Other works have proposed variants of the axisymmetrization mechanism to explain secondary eyewall formation. In addition to the axisymmetrization of convectively generated vorticity, dynamical regions like stagnation radii or critical radii have been hypothesized as focal points for the absorption of vortex Rossby wave activity within the vortex [e.g., *Montgomery and Kallenbach*, 1997; *Camp and Montgomery*, 2001; *Terwey and Montgomery*, 2003]. The question as to whether sheared vortex Rossby waves or inertia-gravity waves dominate the advective dynamics outside the hurricane core has been recently answered using an objective method of identification of the principal asymmetric wave structures [*Brunet*, 1994; *Chen et al.*, 2003]. This method, termed the Empirical Normal Mode Method, has been utilized in high-resolution hurricane simulations to show that the sheared spiral bands outside the primary eyewall are composed primarily of sheared vortex Rossby waves [*Chen and Yau*, 2001; *Chen et al.*, 2003].

[37] Whereas the above dynamical works have contributed important understanding of vorticity axisymmetrization in hurricane-like vortices, these studies have not addressed two aspects of realistic hurricane flows that can arrest the vortex axisymmetrization process. In full-physics numerical simulations like ours, for example, convectively generated vorticity anomalies outside the primary eyewall are of comparable magnitude to the mean vorticity of the eyewall region. These large vorticity amplitudes are not unexpected since convective updrafts tilt the ample horizontal vorticity of the mean hurricane wind field into the vertical, leading to strong dipolar vorticity structures, and stretch the background vertical vorticity [e.g., M06, *Franklin et al.*,

Table 1. List of Secondary Eyewall Formation Hypotheses With Summary of Relevance to our Modeled Hurricanes[a]

Authors	Hypothesis Summary	Relevance to Current Model Results	Type
Willoughby et al. [1982] borrowing from the squall line research of *Zipser* [1977]	Downdrafts from the primary eyewall force a ring of convective updrafts.	Few downdraft-forced updrafts during this time in the simulations.	O
Willoughby [1979]	Internal resonance between local inertia period and asymmetric friction due to storm motion.	No systematic storm motion in the simulated storms.	A
Hawkins [1983]	Topographic effects	No topographic forcing in the simulations.	O
Willoughby et al. [1984]	Ice microphysics	"Warm-rain" (no-ice) sensitivity case also produces secondary eyewall.	A
Molinari and Skubis [1985] and *Molinari and Vallaro* [1989]	Synoptic-scale forcings (e.g., inflow surges, upper-level momentum fluxes)	No synoptic-scale forcings in the simulations	O
Montgomery and Kallenbach [1997], *Camp and Montgomery* [2001] and *Terwey and Montgomery* [2003]	Internal dynamics-axisymmetrization via sheared vortex Rossby wave processes; collection of wave energy near stagnation or critical radii	Possible explanation	N
Nong and Emanuel [2003]	Sustained eddy momentum fluxes and WISHE feedback	Possible explanation	A
Kuo et al. [2004, 2008]	Axisymmetrization of positive vorticity perturbations around a strong and tight core of vorticity.	Possible explanation	N

[a]The type column refers to the type of model or observations that were used to formulate the hypothesis. O stands for observationally-based; A stands for axisymmetric model; N stands for nonaxisymmetric model.

2006]. Such localized vorticity anomalies possess small horizontal scales in comparison to the characteristic diameter of the hurricane eyewall region. The large amplitudes and small scales of the convectively generated vorticity anomalies act to resist axisymmetrization by the larger-scale hurricane vortex [e.g., *Dritschel and Waugh*, 1992; *Enagonio and Montgomery*, 2001].

[38] In a complimentary study, *Rozoff et al.* [2006, hereafter R06] suggested that the nonconvective region between the primary and secondary eyewalls (often called the moat) might be strongly influenced by the large vorticity of the hurricane core. *Houze et al.* [2007] found the moat to be developing as a deep layer of strong subsidence. R06 hypothesized that the moat might not just be dominated by subsidence, which tends to produce a "cap" to convective processes, but that this strong filamentation process will tend to shear apart nascent convective cells before they can mature and organize. R06 derived the timescale associated with the straining portion of the flow, denoted here as τ_{fil}. For a variety of candidate mean vortex profiles, they compared this kinematic timescale to a suitable convective lifetime (approximately 30 min) to determine the potential extent of the moat region by their theory and found it to be consistent with observations of the moat.

[39] The moat and secondary eyewalls are related in that one cannot be collocated with the other. The moat is defined by the lack of deep convection, while the secondary eyewall is defined by the presence of deep convection. We therefore suspect a relationship between the filamentation timescale and secondary eyewall formation in which a secondary eyewall may only form where τ_{fil} is large enough to allow nascent convection to mature and organize. Additionally, we suspect that an additional relationship between secondary eyewall formation and convective available potential energy (CAPE) may be important.

4.2. Quasi Two-Dimensional Turbulence Theory Revisited

[40] Because of the implied role of convection in the secondary eyewall formation process, we now focus on the characteristics of the individual convective cells in the environment of the modeled hurricane. Inspection of the model data sets indicates that these cells have a substantially smaller horizontal spatial scale than the inner core of the hurricane. Considering the potential role of small-scale processes in a rapidly rotating vortex like a hurricane, little inspiration is needed to hypothesize that the convection may be feeding energy into the larger-scale vortex system [cf. *Carr and Williams*, 1989; *Montgomery and Enagonio*, 1998; *McWilliams*, 2006]. The crux of this approach is then determining the fate of this turbulent energy forced by the convective motions, determining where in the hurricane vortex this energy is input, and explaining the factors influencing the frequency and strength of this convection.

[41] Since turbulent flows are generally influenced strongly by dimensionality and intrinsic parameters, we first inquire as to which turbulence theory is most appropriate to build upon for the secondary eyewall problem. Because of their rapidly rotating core and small aspect ratio on the system scale, mature hurricanes evolve largely in a quasi two-dimensional manner [*Shapiro and Montgomery*, 1993; *Montgomery and Shapiro*, 1995; *Montgomery and Kallenbach*, 1997; *Braun et al.*, 2006; *Schecter and Montgomery*, 2007]. On the basis of this aforementioned work, we henceforth assume that the mesoscale circulations generated by the convection in the mature hurricane are constrained approximately by quasi two-dimensional balanced dynamics. A cursory application of two-dimensional turbulence theory [e.g., *Kraichnan*, 1967; *Frisch*, 1996; *McWilliams*, 2006] suggests that
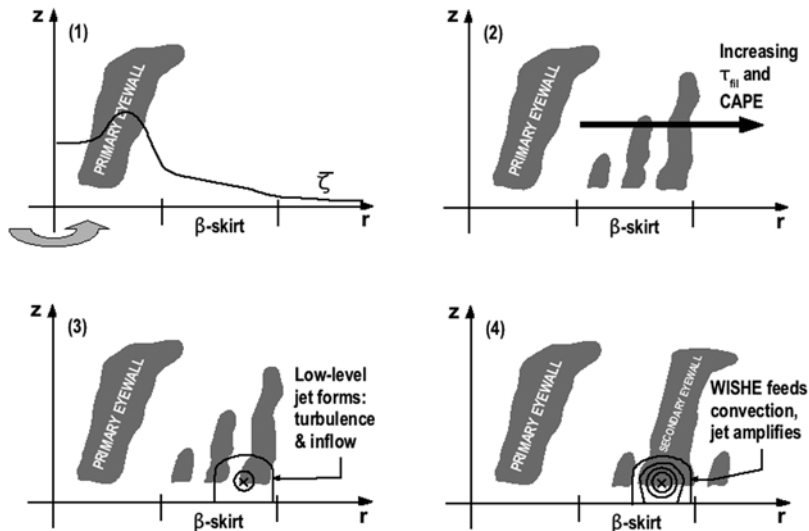
Figure 6. Proposed conceptual model of the β-skirt axisymmetrization (BSA) mechanism for the formation of a secondary eyewall.

energy generated by the convection will tend to cascade upscale while the enstrophy will tend to cascade downscale. Moreover, two-dimensional turbulence calculations on a sphere and on a β-plane have shown that zonal jets form spontaneously from well-stirred initial conditions [*Vallis and Maltrud*, 1993; *Huang and Robinson*, 1998].

[42] The validity of quasi two-dimensional turbulence theory and, therefore, the overriding dynamical framework in which the convective energy and vorticity is input depends strongly on the vorticity structure of the mean hurricane profile. By compositing observations from many mature hurricanes, *Mallen et al.* [2005] showed that fully developed hurricanes typically have a "skirt" of vertical vorticity outside the main core. This "skirt" is where a relatively weak but persistently nonzero radial gradient exists in the azimuthal mean vorticity. Characteristically, the spatial change of background vorticity in a fluid system is referred to as beta. Here the radial gradient of the azimuthal mean (potential) vorticity represents the beta of the hurricane vortex.

[43] The skirt region of a hurricane vortex therefore serves as an area of effective beta where the quasi two-dimensional fluid dynamical processes may be operative when subject to perturbative input from the convective cells. Additionally, mean vorticity gradients tend to stabilize the axisymmetrization process by constraining finite amplitude perturbations to act in a quasi-linear manner when the dynamics would otherwise tend to be arrested by the formation of nonlinear vortex substructures [*Brunet and Montgomery*, 2002; *Montgomery and Brunet*, 2002]. It is from this viewpoint that we propose the following secondary eyewall formation hypothesis for testing.

4.3. Hypothesis

[44] Figure 6 is a conceptual drawing of our secondary eyewall formation theory. To begin with, we envision that the storm includes a spatially extensive skirt of azimuthal mean vertical vorticity with a persistently negative radial gradient in the lower troposphere spanning the inflow layer. This is a general structural feature of mature tropical cyclo-

nes, as *Mallen et al.* [2005] have shown in their composite study of hurricane wind profiles. This skirt of vorticity gently decays to near-zero values as one moves outward toward the far-field environment. Within the skirt region, it is hypothesized that there is a non-trivial effective beta, prompting the nomenclature of "β-skirt" for this area. The actual value of this vorticity gradient may be very small compared to the gradients near the primary eyewall, but even a weak vorticity gradient can have significant dynamical effects.

[45] Within the β-skirt, sporadic convection will form. However, this convection is constrained by many factors. It is readily verified that for realistic hurricane-like wind profiles the mean filamentation timescale, τ_{fil}, increases radially outward. Additionally, observations show that, in major hurricanes, convective available potential energy (CAPE) increases radially outward from the inner-core, often reaching an equilibrium value just outside the primary eyewall [e.g., *Gray and Shea*, 1973; *Frank*, 1977]. These factors together help dictate where deep convection could readily occur. CAPE [*Emanuel*, 1994] is a measure of the amount of energy available to a parcel to convect. Convective inhibition is the amount of energy needed to break through the thermodynamic barrier that is preventing spontaneous convection. Together, these three measures (τ_{fil}, CAPE, convective inhibition) provide information on the convective potential of the region outside the inner-core of the hurricane. If an area of convective potential exists within the β-skirt (e.g., $\tau_{fil} > 30$ min, sufficient CAPE, low convective inhibition), deep convection should be able to form regularly

[46] This convection then acts as a source of perturbation eddy kinetic energy and vorticity in the β-skirt. Given that the horizontal scale of these individual convective cells (typically on the order of 10 km) is small compared to the radial extent of the β-skirt (typically 50 to 100 km radius), the eddy kinetic energy will tend to be fed into the system-scale vortex at small scales.

[47] As one might anticipate from two-dimensional β-plane turbulence theory [*Vallis and Maltrud*, 1993], the

energy from these perturbations will be directed upscale in an anisotropic manner as quasi-zonal jets ("axisymmetrized" into the mean flow) whose widths scale as the beta length scale: $[u_{rms}/\beta]^{1/2}$, where u_{rms} is the root mean squared velocity perturbation and β is the suitably normalized radial derivative of the potential vorticity of the mean hurricane vortex as defined below. These turbulence theories alone, though, do not ensure that the axisymmetrization process will ensue. As previously discussed, the vorticity perturbations generated by the convection are typically as strong as the mean vorticity in the core of the hurricane. Nonlinear numerical experiments of strong vorticity rings around a core of similar strength vorticity have shown the tendency of these intense rings to form polygonal patterns of strong, steady mesovortices [*Schecter et al.*, 1999; *Kossin and Schubert*, 2001]. Other studies have shown that when the vorticity gradient becomes sufficiently strong compared to the local shear, the linear axisymmetrization process becomes uniformly valid and is effectively stabilized against the nonlinear tendency to arrest this upscale cascade [e.g., *Brunet and Montgomery*, 2002; *Montgomery and Brunet*, 2002]. Such considerations suggest that an important role of the β-skirt is to constrain the asymmetric flow within the β-skirt region to evolve approximately as quasi-linear axisymmetrization dynamics would predict, transferring perturbation vorticity and kinetic energy from sporadic deep convection into the azimuthal mean flow. After sufficient time is given for these processes to transfer perturbation vorticity and energy into the mean swirling winds, sporadic deep convection will tend to form a substantial low-level jet in the β-skirt.

[48] An approximate boundary where linear axisymmetrization theory remains a useful first approximation is dependent on the vortex beta Rossby number [e.g., *Möller and Montgomery*, 2000; *Montgomery and Brunet*, 2002]. The vortex beta Rossby number is defined as $[(u_{rms})/(L^2\beta)]$, where L is the eddy length scale. When this number is less than unity, linear dynamics broadly serves as a valid first approximation. Since our eddy velocity scale is essentially linked with the horizontal velocity scale associated with the convection, we see that when the beta scale length is on the same order of magnitude as the convective scale length, linear axisymmetrization dynamics will tend to prevail within the β-skirt. Thus if the axisymmetrization process is to occur, we require sufficient effective beta so that the convective disturbances will tend to be axisymmetrized.

[49] Our β-skirt axisymmetrization (BSA) formation hypothesis is similar to the other internal dynamical formation hypotheses in that perturbations are dynamically forced into the azimuthal mean profile of the hurricane. However, here, the convection is modeled not as an initial value of vorticity or energy, but instead as a persistent and stochastic forcing of the system. Our hypothesis highlights the importance of the β-skirt in helping stabilize the axisymmetrization tendency of the convective forcing, which in turn induces localized jets in the lower troposphere.

[50] In addition to the axisymmetrization of the perturbation kinetic energy, the increased convective activity forces stronger mean low-level inflow from outside this convective region of the tropical cyclone. This inflow supplies additional moisture and latent heat to the nascent secondary eyewall, and also concentrates angular momentum, augmenting the acceleration of the mean low-level jet.

[51] Once a substantial low-level jet forms, it can intensify by coupling with the boundary layer through a wind-induced moisture feedback process such as WISHE [*Nong and Emanuel*, 2003]. In the WISHE model, the increased winds increase the amount of latent and sensible heat fluxes from the ocean surface, which makes the low-level air more convectively favorable. This air begins to form additional strong convective updrafts near or within the azimuthal mean jet, creating a positive feedback loop. This amplifying ring of convection becomes the secondary eyewall.

[52] One virtue of the BSA hypothesis is that it can be tested and used operationally with current hurricane observational methods. Accurate azimuthal mean wind profiles can be computed from dropsonde and aircraft measurements. Radial wind profiles can be examined for the existence of a sufficient low-level β-skirt region with large filamentation timescales. Dropsondes can also be used to compute the convective potential in that region, ensuring that convective inhibition is low enough to allow for frequent convection.

5. Supporting Model Evidence

[53] To test the proposed BSA hypothesis, we now present evidence from our control simulation. As stated previously, we will be focusing on the formation period, defined as Hours 8 to 18.

[54] Figure 7 shows calculations of effective β and τ_{fil}, using temporally averaged azimuthal mean flow quantities over a 4-h period from Hour 8 to Hour 12. Temporal averaging is used to reduce the small-scale noise from phenomena like convective processes and show the representative mean waveguide in which the perturbations evolve. Rather than using a basic definition of β as the radial derivative of vorticity, we utilize a definition that better takes into account the unique dynamical constraints of the hurricane vortex. Effective β is defined from the asymmetric balance theories of *Shapiro and Montgomery* [1993] and *Montgomery and Kallenbach* [1997] for a one-layer barotropic fluid as $(-\partial\langle q\rangle/\partial r)(\langle\xi\rangle/\langle q\rangle)$, where q is the Ertel potential vorticity, $\xi = f_0 + 2v_t/r$ is the modified Coriolis parameter, v_t is the mean tangential velocity, and $\langle F\rangle$ indicates a temporal and azimuthal average of the quantity F. The negative sign on effective β is used such that the increase in potential vorticity with decreasing radius is associated with positive β. This convention allows standard β-plane and spherical thinking to be applied in regions with radially decreasing potential vorticity. For τ_{fil}, we use the azimuthal averaged version from R06, defined as $\tau_{fil} = [-(\langle v_t\rangle/r)(\partial\langle v_t\rangle/\partial r)]^{-1/2}$.

[55] From Figure 7 we see that there is a low-level β-skirt during these four hours. The value of β in the skirt is strictly positive below 1 km out to a radius of 125 km. Prior to Hour 0, we note that the β-skirt does not extend far out from the inner-core (Figure 8), barely reaching out to more than 80 km radius from Hours -12 to -8.

[56] Borrowing from basic β-plane turbulence theories [e.g., *Vallis and Maltrud*, 1993], the effective beta scale length suggests that this skirt will tend to force jets with radial scales larger than, but with the similar magnitude as,
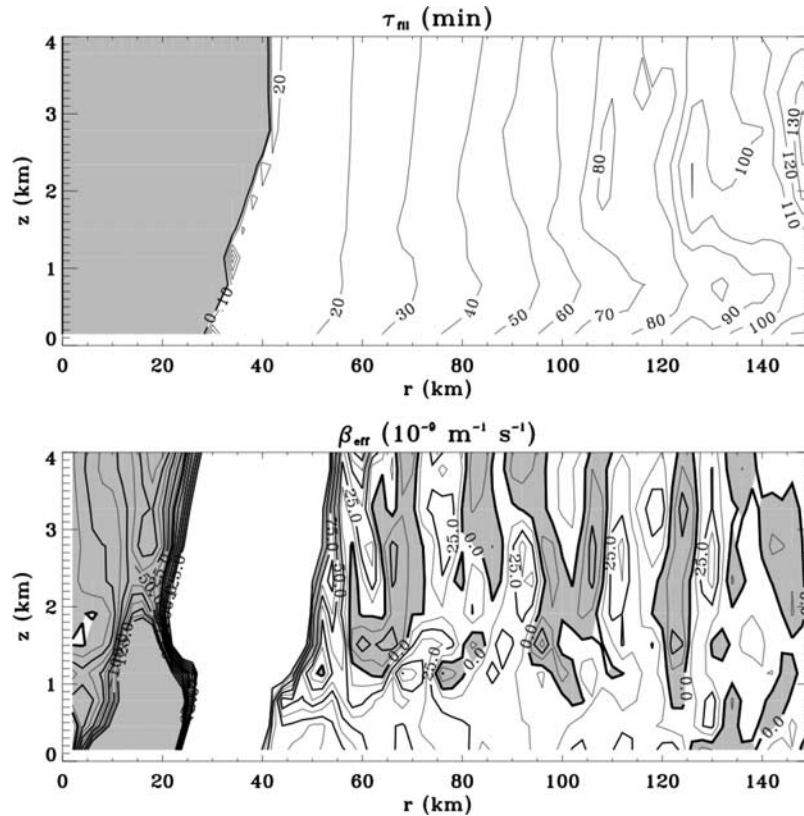
Figure 7. Calculations of $\tau_{\rm fil}$ and effective β in the control simulation. This calculation uses temporally averaged azimuthal mean quantities from Hours 8 to 12. Contour intervals are 10 min for $\tau_{\rm fil}$ and 12.5×10^{-9} m^{-1} s^{-1} for β. Negative β and vorticity-dominated regions for $\tau_{\rm fil}$ are shaded. Only the first ten contours of each sign are plotted for β.

$[u_{\rm rms}/\beta]^{1/2}$, where $u_{\rm rms}$ is the root-mean squared horizontal eddy velocity perturbation. Within our β-skirt after Hour 0, this effective beta scale comes out as 12 to 24 km, given that the root mean squared velocity perturbations are diagnosed to be 4 to 7 m s^{-1} and β is diagnosed to be 12.5 to 25×10^{-9} m^2 s^{-2} in this region. The beta timescale for this process, $[\beta\, u_{\rm rms}]^{-1/2}$, is on the order of 40 to 75 min. If we assume that the eddy length scale is approximately 20 km, the vortex beta Rossby number, $[(u_{\rm rms})/(L^2\beta)]$, is estimated to be on the order of 0.36 to 1.44, suggesting that the perturbations of these scales generated in the β-skirt should be approximately governed by quasi-linear dynamics and, hence, axisymmetrized in time.

[57] From Figure 7, we see that, as expected, the mean filamentation timescale increases with radius. R06 suggested that $\tau_{\rm fil}$ greater than 30 min would be sufficient to allow convection to grow before the straining process disrupts the updraft. The region with $\tau_{\rm fil}$ greater than 30 min stretches from 70 km radius outward. Therefore we expect that any convection that forms during and after this period outside of 70 km radius may be potentially deep and long-lived according to the filamentation dynamics.

[58] Examining the azimuthal mean soundings for thermodynamic considerations, we also note that the mean surface-based CAPE in the region from 60 km to 200 km is 900 to 1100 J kg^{-1} with very low convective inhibition (CIN) of 0 to 2 J kg^{-1} (not shown). These values change very little during the formation period, having settled into these equilibrium values during the rapid intensification period prior to Hour 0. Within such a convectively favorable environment, we expect convective activity to be robust in the region outside of 70 km. Our model suggests that, if a secondary eyewall were to form by the processes outlined in our hypothesis, it should occur where the β-skirt overlaps with a convectively favorable region. In the control simulation, we have identified this overlap region to be between 70 and 125 km in radius.

[59] At earlier times, $\tau_{\rm fil}$ is not significantly different from what is seen between Hours 8 and 12 (Figure 7). Thus as we can see from Figure 8, the overlap region between the β-skirt and the convectively favorable region is virtually nonexistent between Hours -24 and -20 and very narrow (approximately $10-15$ km radius) between Hours -12 and -8. Given that there were no observed secondary eyewall formations in the control simulation prior to Hour 0, this observation gives further support to our hypothesis that the β-skirt is an integral part of the secondary eyewall formation process.

[60] In our BSA hypothesis, the convection acts as a source of small-scale eddy kinetic energy in the β-skirt. To examine the kinetic energy cascade, we separate the kinetic energy into its mean flow and perturbation components and then calculate the Fourier power of the perturbation energy in azimuthal wave number space. We first interpolate the data from a Cartesian grid onto a cylindrical grid with 200 radial grid points at 2 km grid spacing and 210 azimuthal
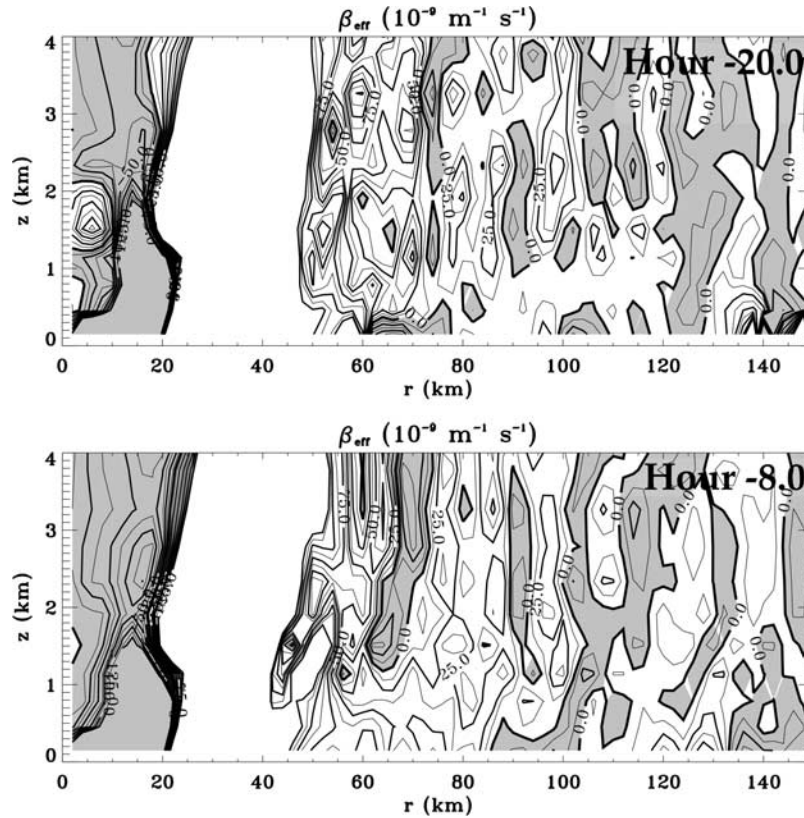
Figure 8. Effective β for times prior to Hour 0. The top frame utilizes temporally and azimuthally averaged quantities over the four hours between Hours -24 and -20. The bottom frame utilizes quantities averaged over the four hours between Hours -12 and -8. Contours and shading as in Figure 7.

grid points. Integrating the kinetic energy in the region of the model between 60 and 150 km radius and 0 to 4 km height and weighting the integral by the mean density, we are able to approximately determine the spatial scales of the kinetic energy perturbations. Figure 9 shows the results of this calculation at three times during the secondary eyewall formation period.

[61] Between Hours 8 and 16, there is a gradual increase in kinetic energy throughout the majority of the spectrum. The Hour 16 energy spectrum is approximately $30-60\%$ greater than the Hour 8 spectrum at each azimuthal wave number. This increase supports the hypothesis that, in the candidate secondary eyewall formation region, there is a source of perturbation kinetic energy. We suggest that this source is increased convective activity in this region.

[62] To show the increase in convective activity as well as the formation of a low-level jet structure, we examine the colocation of mean variance of perturbation vertical velocity with changes in the mean tangential wind during the formation period. Since it is easier to see small changes to a large mean field like tangential winds by examining the field as a difference from a reference field, we define $\Delta v(r, z)$ as the change in the mean tangential winds from Hour 0.

[63] Figure 10 shows the Δv and azimuthally averaged variance of the perturbation vertical velocity (w'^2) calculations between 0 and 200 km radius and 0 and 4 km height for four times during the secondary eyewall formation period: Hours 7, 9, 11, and 13. From Hours 7 to 9, we see little change in the mean structure of the hurricane.

There is a small increase of approximately 1 m s^{-1} outside of 150 km radius around 1 km height during this time. However, during the next two hours, we see an increase of mean tangential winds by 3 to 5 m s^{-1} from 70 km to 150 km through the lowest layers of the model. The spatial scale of this cyclonic jet is approximately 40 to 60 km, which is quantitatively larger than the estimated beta length scale of 12 to 24 km. Additionally, the jet formed mainly within the overlap region we identified earlier.

[64] The formation of the localized jet is coupled with significant activity in the vertical motion fields, as evidenced by the solid contour in Figure 10, which denotes the 1 m^2 s^{-2} contour of the azimuthally averaged variance of the perturbation vertical velocity (w'^2). Since strong hurricane convection has been shown to have local values of w' with values around 10 m s^{-1} [e.g., *Braun*, 2002; *Braun et al.*, 2006; *Marks et al.*, 2008], an azimuthal mean contour of 1 m^2 s^{-2} indicates that there are nontrivial amounts of vertical motion associated with deep convective processes occurring in that annular region. From Figure 10, we note the continual increase in the spatial coverage of the 1 m^2 s^{-2} contour, in particular, directly above where the jet forms (in Hour 9) and just above the entirety of the jet (in Hour 13). The former shows that convective activity was increasing prior to the strengthening of the jet. The latter is consistent with the potential feedback mechanism of WISHE in forcing convection in response to the formation of a low-level jet.
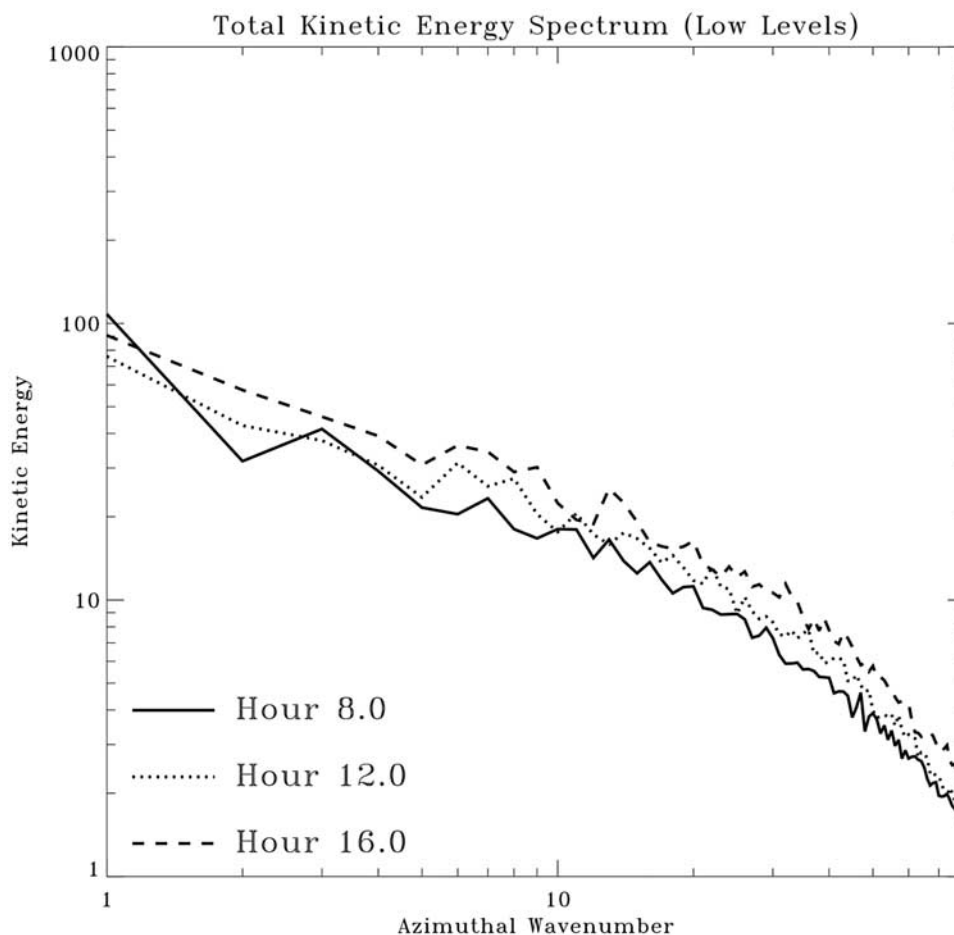
Figure 9. Low-level (0 to 4 km height) perturbation kinetic energy spectrum for three different times during the secondary eyewall formation period for the control experiment, calculated in an annulus from 60 to 150 km in radius. Units for kinetic energy are m^2 s^{-2}.

[65] The low-level inflow during this time period also increases appreciably. The mean radial wind speed increases approximately 1 to 4 m s^{-1} between Hours 8 and 10 outside of 100 km radius and below 3 km height (not shown).

[66] Assembling the evidence thus far, we see that the simulated secondary eyewall formation is consistent with the proposed BSA hypothesis. During the time period where there is an overlap of a sufficiently strong low-level β-skirt and favorable convective profiles, we observe an increase in perturbation kinetic energy at almost all azimuthal wave numbers. The kinetic energy increase at high azimuthal wave numbers and the increase in mean vertical velocity variance suggest that deep convective activity is increasing on relatively small (hot tower) scales. Following the increase in eddy kinetic energy, we observe a low-level jet form and strengthen. Given the increased convective activity and the fact that the nonlinear axisymmetrization mechanism in the β-skirt would tend to force a jet with a characteristic radial scale of tens of kilometers, commensurate with the beta scale, we suggest here that the β-skirt hypothesis is a very plausible explanation. The observation that the jet forms on the timescale of a few hours (e.g., Figure 10) gives additional support to the BSA hypothesis since the associated timescale (the beta timescale) for

perturbations to be influenced by the β-skirt is approximately 40 to 75 min.

6. No-Ice Sensitivity Case

[67] In the following sensitivity experiment, we use the same model setup as the control simulation, except that we turn off all of the ice species. Overall, the evolution of this storm is very similar to the control case. Maximum tangential winds are generally 5 to 10 m s^{-1} less in the no-ice case than in the control simulation, and there is a slightly higher central pressure.

[68] As we see in Figure 11, this sensitivity experiment also underwent a secondary eyewall cycle. In the accompanying figures for the no-ice experiment, Hour 0 is set at 168 h into the simulation, indicating a slight delay in the secondary eyewall cycle by approximately 12 h compared with the control simulation.

[69] We note that the primary eyewall in the no ice experiment is somewhat more diffuse in the azimuthal mean than the control experiment. This is because the primary eyewall in the no ice experiment is generally less circular, tending toward polygonal and elliptical shapes even during the storm's peak intensity period (not shown). In this experiment, the secondary eyewall begins forming around Hour 12, completely circling the inner eyewall around
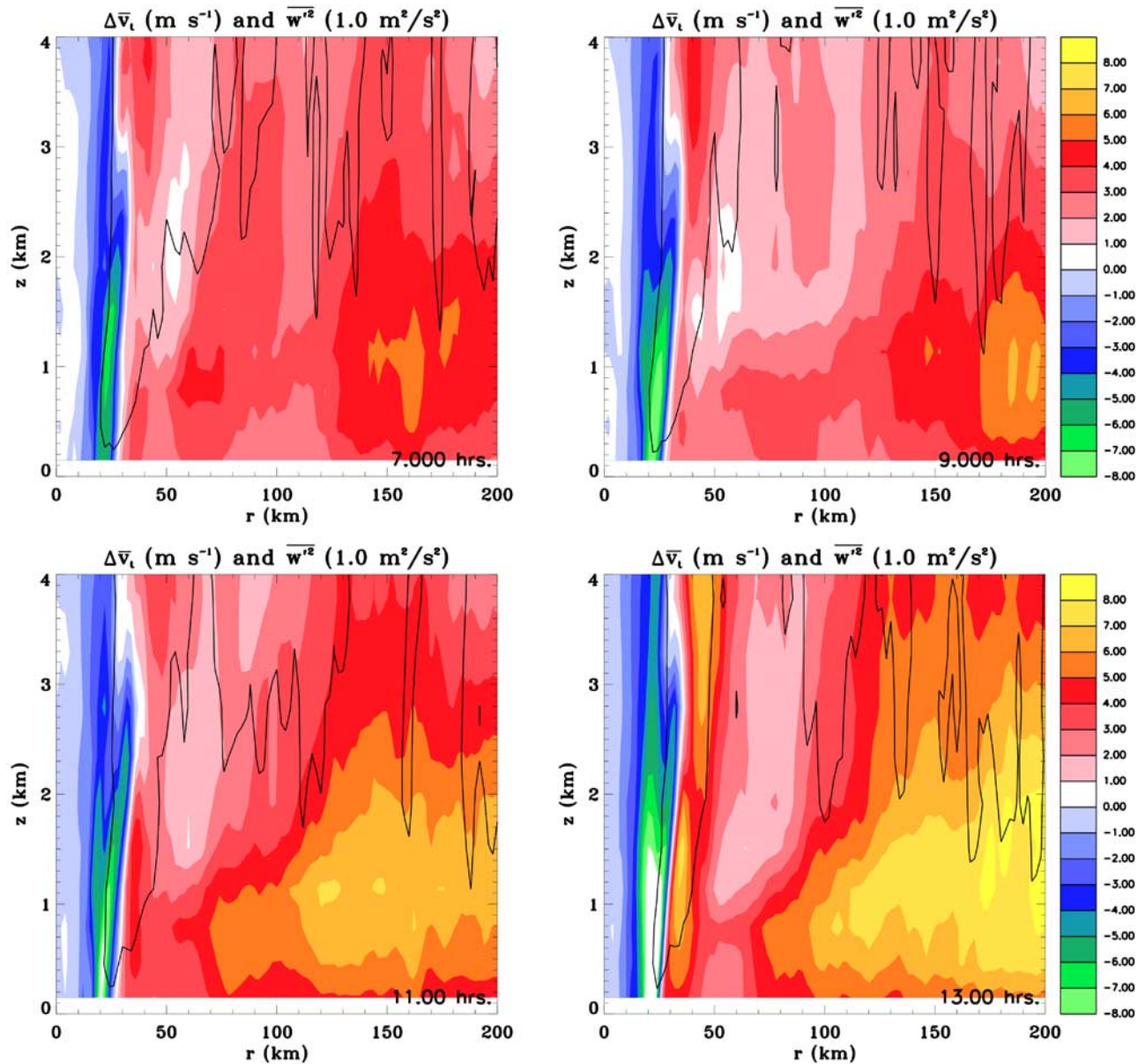
Figure 10. Change in mean tangential wind (shaded, m s^{-1}) from Hour 0, along with the instantaneous mean w$'^2$ contour of 1 m^2 s^{-2} in thick black from the control experiment. Calculations for Hour 7 (top left), Hour 9 (top right), Hour 11 (bottom left), and Hour 13 (bottom right) show the intensification of a low-level jet.

Hours 15 to 16. We note that the primary eyewall decays completely during this 24-h period, disappearing from Figure 11 by Hour 21 as the secondary eyewall strengthens and contracts.

[70] We begin the examination of this experiment's secondary eyewall formation by looking for the presence of a β-skirt. Figure 12 shows the four-hour averaged β-skirt and τ_{fil} calculations for Hours 5 to 9. The existence of a positive β-skirt out to 110 km radius is clearly evident. Additionally, τ_{fil} is greater than 30 min outside of a radius of 75 km. From the BSA hypothesis, then, we would expect that, if there were a secondary eyewall formation, it would occur between 75 and 110 km radius, assuming that the thermodynamics are also favorable in this region. Mean soundings show a surface-based CAPE of 1200 to 1500 J kg^{-1} outside

of 70 km, with generally small (0 to 4 J kg^{-1}) values of CIN (not shown). Looking back at Figure 11, we see that the first significant convection that eventually forms the secondary eyewall occurs around Hours 12 to 13 and at radius 80 to 110 km.

[71] As with the control simulation, we also see the formation of a low-level jet a few hours before the secondary eyewall is fully formed. Figure 13 shows the change in the mean tangential velocity from Hour 0 for four times during the formation period in the no-ice experiment. We see a similar evolution as in Figure 10, where a jet forms rather quickly. The change in the mean swirling flow between Hours 6 and 10 is approximately 4 to 6 m s^{-1}. Additionally, there appears to be more significant convective activity during this period as the coverage of the 1 m^2 s^{-2} heating
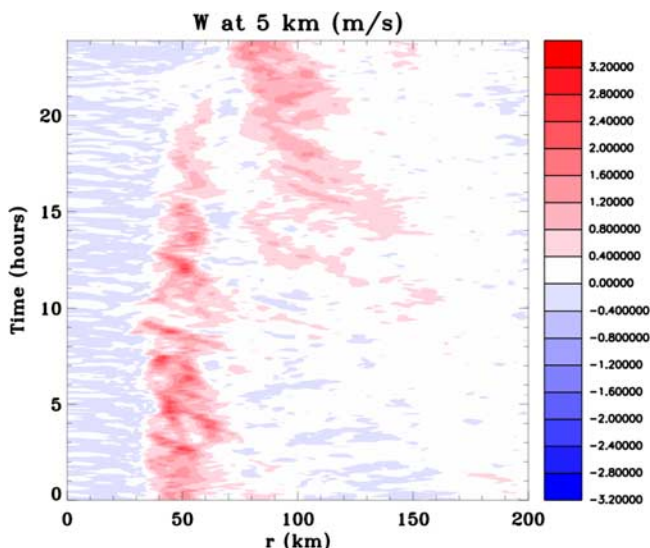
Figure 11. Time-radius plot of azimuthal mean vertical velocity (m s^{-1}) at 5 km height in the no-ice experiment.

contour increases. Last, there is an increase of 1 to 3 m s^{-1} in the mean radial low-level inflow just outside the secondary eyewall formation region between Hours 8 and 10.

7. Discussion and Conclusions

[72] The formation of a secondary eyewall is one of the most important problems in the forecasting of mature

hurricane intensity. A number of different hypotheses by other scientists have been offered to explain this feature, although most of these have been shown to be unnecessary in the formation of our simulated secondary eyewalls. Unsatisfied by the lack of a comprehensive hypothesis and supporting theoretical ideas from previous authors for the secondary eyewall formation problem, we have employed idealized full-physics hurricane simulations to offer a new hypothesis on the formation process.

[73] The beta-skirt axisymmetrization (BSA) formation hypothesis begins with an updated view of a mature tropical cyclone structure, one with a low-level β-skirt as seen in composite observations [*Mallen et al.*, 2005]. If there is a substantial overlap between this β-skirt and an area of strong convective potential (i.e., large filamentation time-scales, sufficient CAPE, and low CIN), we envision that convection will readily form and be sustained for some time in this region. Cumulus convective activity acts as a source of eddy vorticity that, in the presence of a sufficiently well developed β-skirt, will tend to generate one or more localized cyclonic jet maxima possessing a radial scale on the order of the local beta scale. In the hurricane problem, an equivalent barotropic mean radial potential vorticity gradient is substituted for the meridional gradient of planetary vorticity originally utilized for large-scale oceanic and atmospheric flows. Cumulus convective activity also aids in the formation of the low-level jet by forcing additional low-level inflow into the formation region, which converges cyclonic vorticity from the system-scale (parent) vortex. Upon coupling with the boundary layer via sensible and
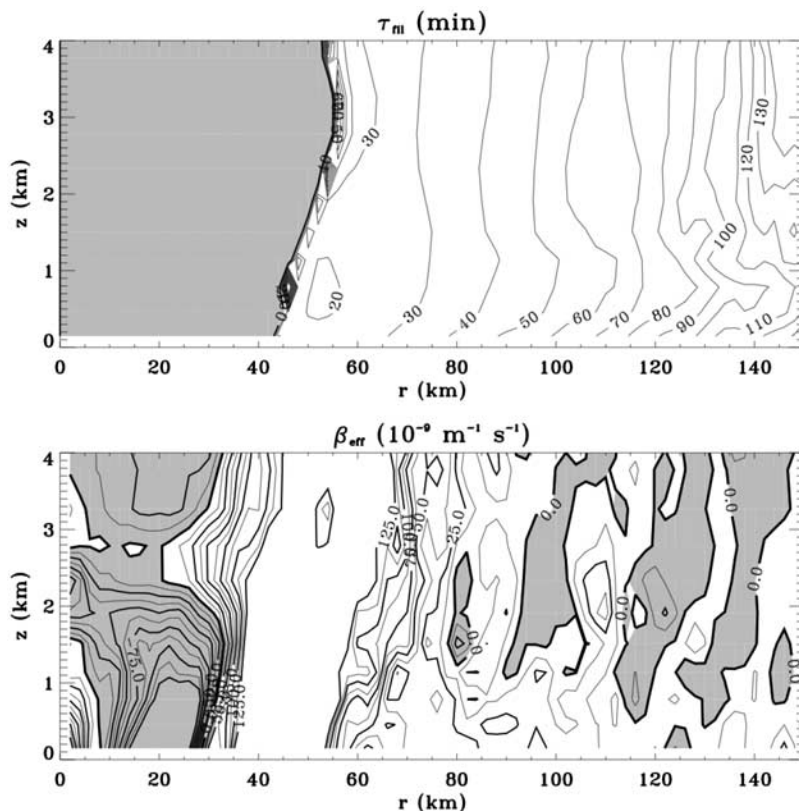

Figure 12. Calculations of the effective β and τ_{fil} in the no-ice experiment. This calculation uses temporally averaged azimuthal mean quantities from Hours 5 to 9. Contours and shading as in Figure 7.
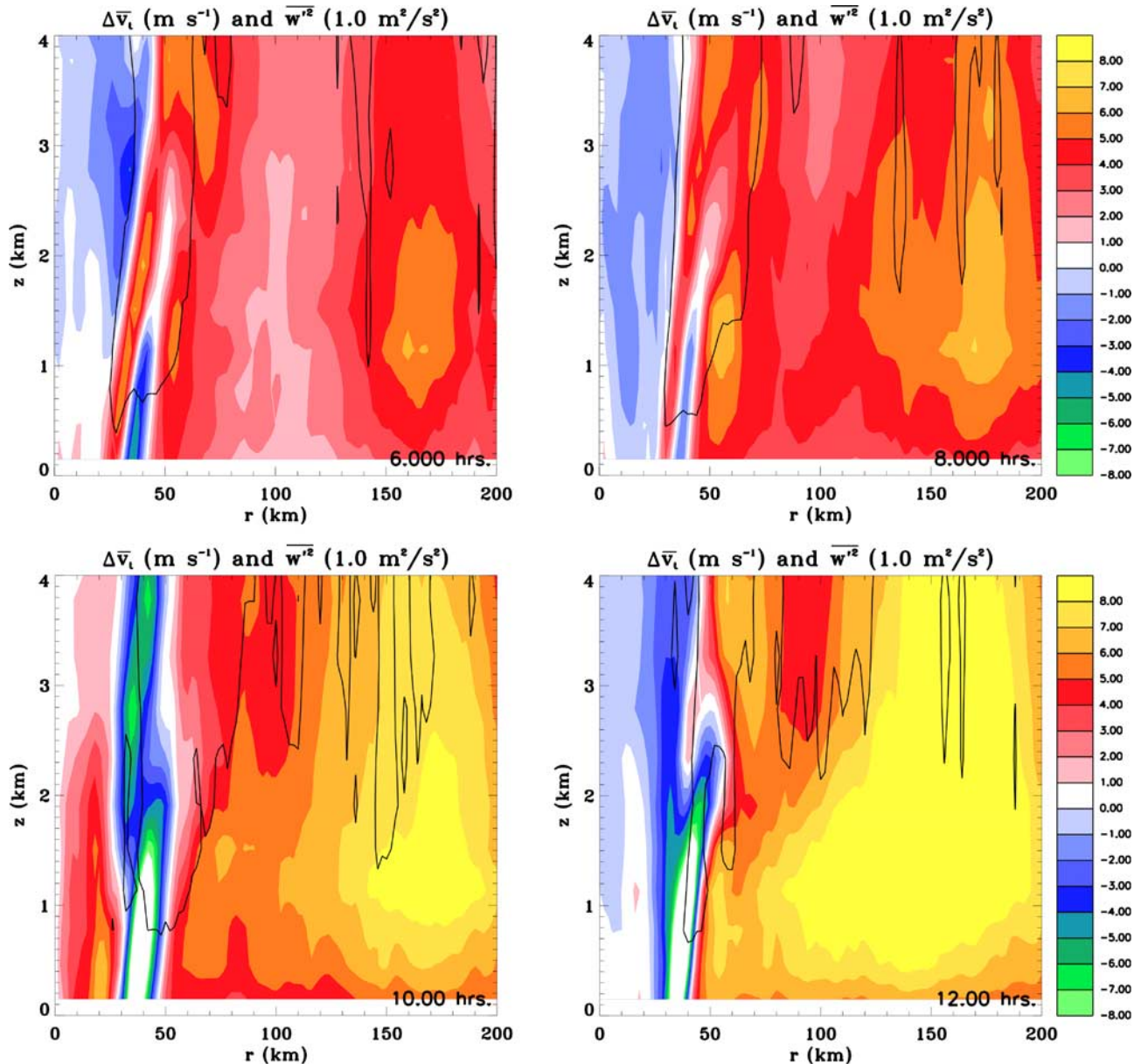
Figure 13. Change in mean tangential wind (m s^{-1}) from Hour 0 in the no-ice experiment, along with the instantaneous mean $\overline{w'^2}$ contour of 1 m^2 s^{-2} in thick black. Calculations for Hour 4 (top left), Hour 6 (top right), Hour 8 (bottom left), and Hour 10 (bottom right) are shown. Contours and shading as in Figure 10.

latent heat exchanges from the ocean surface, the induced jet can then amplify to force additional cumulus convection.

[74] Using our high-resolution and long-time hurricane simulations, we show supporting evidence that this process may be occurring in the model atmosphere. Hours before the secondary eyewall forms, we observe the formation of a well-defined β-skirt, as well as an overlap region where convection is not significantly hindered by weak thermodynamics or strong straining dynamics from the primary swirling flow. In this overlap region, we see an increase in perturbation kinetic energy and convection, along with the formation of a low-level jet that within a few hours amplifies into a secondary eyewall.

[75] Since we have shown that similar results are found without ice microphysical processes, we conclude that the basic dynamics of this process is not essentially dependant on ice microphysics.

[76] Additionally, given the lack of secondary eyewall formations in established axisymmetric models without additional parameterized physics like eddy momentum fluxes [*Rotunno and Emanuel*, 1987; *Emanuel*, 1995; *Nong and Emanuel*, 2003], we suggest that the formation of the secondary eyewall may be controlled by asymmetric processes such as our hypothesized BSA formation process.

[77] Additional future work is planned to test this theory and to gauge the operational usefulness of this hypothesis by including posteriori analyses of observational hurricane data sets where secondary eyewalls have been observed to form.

References

Bister, M., and K. A. Emanuel (1997), The genesis of Hurricane Guillermo: TEXMEX analyses and a modeling study, *Mon. Weather Rev.*, *125*, 2662–2682.

Black, M. L., and H. E. Willoughby (1992), The concentric eyewall cycle of Hurricane Gilbert, *Mon. Weather Rev.*, *120*, 947–957.

Braun, S. A. (2002), A cloud-resolving simulation of Hurricane Bob (1991): Storm structure and eyewall buoyancy, *Mon. Weather Rev.*, *130*, 1573–1592.

Braun, S. A., M. T. Montgomery, and Z. Pu (2006), High-resolution simulation of Hurricane Bonnie (1998). Part I: The organization of eyewall vertical motion, *J. Atmos. Sci.*, *63*, 19–42.

Brunet, G. (1994), Empirical normal-mode analysis of atmospheric data, *J. Atmos. Sci.*, *51*, 932–952.

Brunet, G., and M. T. Montgomery (2002), Vortex Rossby waves on smooth circular vortices. Part I: Theory, *Dyn. Atmos. Ocean.*, *35*, 153–177.

Camp, J. P., and M. T. Montgomery (2001), Hurricane maximum intensity: Past and present, *Mon. Weather Rev.*, *129*, 1704–1717.

Carr, L. E., and R. T. Williams (1989), Barotropic vortex stability to perturbations from axisymmetry, *J. Atmos. Sci.*, *46*, 3177–3191.

Chen, Y., and M. K. Yau (2001), Spiral bands in a simulated hurricane. part I: Vortex Rossby wave verification, *J. Atmos. Sci.*, *58*, 2128–2145.

Chen, Y., G. Brunet, and M. K. Yau (2003), Spiral bands in a simulated hurricane. Part II: Wave activity diagnostics, *J. Atmos. Sci.*, *60*, 1239–1256.

Clark, T. L., and R. D. Farley (1984), Severe downslope windstorm calculations in two and three spatial dimensions using anelastic grid nesting: A possible mechanism for gustiness, *J. Atmos. Sci.*, *41*, 329–350.

Cotton, W. R., et al. (2003), RAMS 2001: Current status and future directions, *Meteorol. Atmos. Phys.*, *82*, 5–29.

Dodge, P., R. W. Burpee, and F. D. Marks Jr. (1999), The kinematic structure of a hurricane with sea level pressure less than 900 mb, *Mon. Weather Rev.*, *124*, 987–1004.

Dritschel, D. G., and D. W. Waugh (1992), Quantification of the inelastic interaction of unequal vortices in two-dimensional vortex dynamics, *Phys. Fluids*, *A4*, 1737–1744.

Emanuel, K. A. (1989), The finite-amplitude nature of tropical cyclogenesis, *J. Atmos. Sci.*, *46*, 3431–3456.

Emanuel, K. A. (1994), *Atmospheric Convention*, 580 pp., Oxford Univ. Press, Inc., New York.

Emanuel, K. A. (1995), The behavior of a simple hurricane model using a convective scheme based on subcloud-layer entropy equilibrium, *J. Atmos. Sci.*, *52*, 3960–3968.

Enagonio, J. E., and M. T. Montgomery (2001), Tropical cyclogenesis via convectively forced vortex Rossby waves in a shallow water primitive equation model, *J. Atmos. Sci.*, *58*, 685–706.

Frank, W. M. (1977), The structure and energetics of the tropical cyclone. part I: Storm structure, *Mon. Weather Rev.*, *105*, 1119–1135.

Franklin, C. N., G. J. Holland, and P. T. May (2006), Mechanisms for the generation of mesoscale vorticity features in tropical cyclone rainbands, *Mon. Weather Rev.*, *134*, 2649–2669.

Frisch, U. (1996), *Turbulence: The Legacy of A. N. Kolmogorov*, 310 pp., Cambridge Univ. Press, New York.

Gray, W. M., and D. J. Shea (1973), The hurricane's inner core region. Part II: Thermal stability and dynamic characteristics, *J. Atmos. Sci.*, *30*, 1565–1576.

Harrington, J. Y. (1997), The effects of radiative and microphysical processes on simulated warm and transitional season arctic stratus, Ph.D. thesis, 289 pp., Colorado State Univ., Fort Collins, Colo.

Hawkins, H. F. (1983), Hurricane Allen and island obstacles, *J. Atmos. Sci.*, *40*, 1360–1361.

Hawkins, J. D., and M. Helveston (2004), Tropical cyclone multiple eyewall characteristics, *26th Conf. on Hurr. and Trop. Met., Preprints, AMS*, pp. 276–277, Miami, Fla.

Hill, G. E. (1974), Factors controlling the size and spacing of cumulus clouds as revealed by numerical experiments, *J. Atmos. Sci.*, *31*, 646–673.

Houze, R. A., S. Chen, W.-C. Lee, R. Rogers, J. Moore, G. Stossmeisterr, M. Bell, J. Cetrone, W. Zhao, and S. Brodzik (2006), The hurricane rainband and intensity change experiment: Observations and modeling of hurricanes Katrina, Ophelia, and Rita, *Bull. Am. Meteorol. Soc.*, *87*, 1503–1521.

Houze, R. A., S. S. Chen, B. F. Smull, W.-C. Lee, and M. M. Bell (2007), Hurricane intensity and eyewall replacement, *Science*, *315*, 1235–1239.

Huang, H.-P., and W. A. Robinson (1998), Two-dimensional turbulence and persistent zonal jets in a global barotropic model, *J. Atmos. Sci.*, *55*, 611–632.

Jordan, C. L. (1958), Mean soundings for the West Indies area, *J. Meteorol.*, *15*, 91–97.

Kossin, J. P., and W. H. Schubert (2001), Mesovortices, polygonal flow patterns, and rapid pressure falls in hurricane-like vortices, *J. Atmos. Sci.*, *58*, 2196–2209.

Kraichnan, R. H. (1967), Inertial ranges in two-dimensional turbulence, *Phys. Fluids*, *10*, 1417–1423.

Kuo, H.-C., L.-Y. Lin, C.-P. Chang, and R. T. Williams (2004), The formation of concentric vorticity structures in typhoons, *J. Atmos. Sci.*, *61*, 2722–2734.

Kuo, H.-C., W. H. Schubert, C.-L. Tsai, and Y.-F. Kuo (2008), Vortex interactions and the barotropic aspects of concentric eyewall formation, *Mon. Weather Rev.*, *136*, in press.

Lilly, D. K. (1962), On the numerical simulation of buoyant convection, *Tellus, Ser. A and Ser. B*, *14*, 148–172.

Louis, J. F. (1979), A parametric model of vertical eddy fluxes in the atmosphere, *Boundary Layer Meteorol.*, *17*, 187–202.

Mallen, K. J., M. T. Montgomery, and B. Wang (2005), Reexamining the near-core radial structure of the tropical cyclone primary circulation: Implications for vortex resiliency, *J. Atmos. Sci.*, *62*, 408–425.

Marks, F. D., P. B. Black, M. T. Montgomery, and R. W. Burpee (2008), Structure of the eye and eyewall of Hurricane Hugo (1989), *Mon. Weather Rev.*, *136*, 1237–1259.

McWilliams, J. C. (2006), *Fundamentals of Geophysical Fluid Dynamics*, 266 pp., Cambridge Univ. Press, New York.

McWilliams, J. C., and G. R. Flierl (1979), On the evolution of isolated, nonlinear vortices, *J. Phys. Oceanogr.*, *9*, 1155–1182.

Melander, M. V., J. C. McWilliams, and N. J. Zabusky (1987), Axisymmetrization and vorticity-gradient intensification of an isolated two-dimensional vortex through filamentation, *J. Fluid. Mech.*, *178*, 137–159.

Molinari, J., and S. Skubis (1985), Evolution of the surface wind field in an intensifying tropical cyclone, *J. Atmos. Sci.*, *42*, 2856–2879.

Molinari, J., and D. Vallaro (1989), External influences on hurricane intensity. Part I: Outflow layer eddy angular momentum fluxes, *J. Atmos. Sci.*, *46*, 1093–1105.

Möller, J. D., and M. T. Montgomery (2000), Tropical cyclone evolution via potential vorticity anomalies in a three-dimensional balance model, *J. Atmos. Sci.*, *57*, 3366–3387.

Montgomery, M. T., and G. Brunet (2002), Vortex Rossby waves on smooth circular vortices. Part II: Idealized numerical experiments for tropical cyclone and polar vortex interiors, *Dyn. Atmos. Oceans*, *35*, 179–204.

Montgomery, M. T., and J. E. Enagonio (1998), Tropical cyclogenesis via convectively forced vortex Rossby waves in a three-dimensional quasigeostrophic model, *J. Atmos. Sci.*, *57*, 3176–3207.

Montgomery, M. T., and R. J. Kallenbach (1997), A theory for vortex Rossby waves and its application to spiral bands and intensity changes in hurricanes, *Q. J. R. Meteorol. Soc.*, *123*, 435–465.

Montgomery, M. T., and L. J. Shapiro (1995), Generalized Charney-Stern and Fjortoft theorems for rapidly rotating vortices, *J. Atmos. Sci.*, *52*, 1829–1833.

Montgomery, M. T., M. E. Nicholls, T. A. Cram, and A. B. Saunders (2006), A vortical hot tower route to tropical cyclogenesis, *J. Atmos. Soc.*, *63*, 355–386.

Nong, S., and K. Emanuel (2003), A numerical study of the genesis of concentric eyewalls in hurricanes, *Q. J. R. Meteorol. Soc.*, *129*, 3323–3338.

Pielke, R. A., et al. (1992), A comprehensive meteorological modeling system – RAMS, *Meteorol. Atmos. Phys.*, *49*, 69–91.

Raymond, D. L., C. Lopez-Carillo, and L. Lopez Cavazos (1998), Case-studies of developing east Pacific easterly waves, *Q. J. R. Meteorol. Soc.*, *124*, 2005–2034.

Reasor, P. D., M. T. Montgomery, and L. F. Bosart (2005), Mesoscale observations of the genesis of Hurricane Dolly (1996), *J. Atmos. Sci.*, *62*, 3151–3171.

Rotunno, R., and K. A. Emanuel (1987), An air-sea interaction theory for tropical cyclones. part II: Evolutionary study using a nonhydrostatic axisymmetric numerical model, *J. Atmos. Sci.*, *44*, 542–561.

Rozoff, C. M., W. H. Schubert, B. D. McNoldy, and J. P. Kossin (2006), Rapid filamentation zones in intense tropical cyclones, *J. Atmos. Sci.*, *65*, 325–340.

Schecter, D. A., and M. T. Montgomery (2007), Waves in a cloudy vortex, *J. Atmos. Sci.*, *64*, 314–337.

Schecter, D. A., D. H. E. Dubin, K. S. Fine, and C. F. Driscoll (1999), Vortex crystals from 2D flow: Experiment and simulation, *Phys. Fluids*, *11*, 905–914.

Shapiro, L. J. (1992), Hurricane vortex motion and evolution in a three-layer model, *J. Atmos. Sci.*, *49*, 140–154.

Shapiro, L. J., and M. T. Montgomery (1993), A three-dimensional balance theory for rapidly rotating vortices, *J. Atmos. Sci.*, *50*, 3322–3335.

Shapiro, L. J., and H. E. Willoughby (1982), The response of balanced hurricanes to local sources of heat and momentum, *J. Atmos. Sci.*, *39*, 378–394.

Smagorinsky, J. S. (1963), General circulation experiments with the primitive equations. Part I: The basic experiment, *Mon. Weather Rev.*, *91*, 99–164.

Terwey, W. D. and M. T. Montgomery (2003), Vortex waves and evolution in sharp vorticity gradient vortices, Colorado State University Bluebook #734, 97 pp.

Tripoli, G. J., and W. R. Cotton (1981), The use of ice-liquid water potential temperature as a thermodynamic variable in deep atmospheric models, *Mon. Weather Rev.*, *109*, 1094–1102.

Tripoli, G. J., and W. R. Cotton (1982), The Colorado State University three-dimensional cloud/mesoscale model – 1982. Part I: General theoretical framework and sensitivity experiments, *Atmos. Res.*, *16*, 185–220.

Vallis, G. K., and M. E. Maltrud (1993), Generation of mean flows and jets on a beta plane and over topography, *J. Phys. Oceanogr.*, *23*, 1346–1362.

Walko, R. L., W. R. Cotton, J. L. Harrington, and M. P. Myers (1995), New RAMS cloud microphysics parameterization. Part I: The single moment scheme, *Atmos. Res.*, *38*, 29–62.

Willoughby, H. E. (1979), Forced secondary circulations in hurricanes, *J. Geophys. Res.*, *84*, 3173–3183.

Willoughby, H. E., and P. G. Black (1996), Hurricane Andrew in Florida: Dynamics of a disaster, *Bull. Am. Meteorol. Soc.*, *77*, 543–549.

Willoughby, H. E., J. A. Clos, and M. G. Shoreibah (1982), Concentric eye walls, secondary wind maxima, and the evolution of the hurricane vortex, *J. Atmos. Sci.*, *39*, 395–411.

Willoughby, H. E., H.-L. Jin, S. J. Lord, and J. M. Piotrowicz (1984), Hurricane structure and evolution as simulated by an axisymmetric, non-hydrostatic numerical model, *J. Atmos. Sci.*, *41*, 1169–1186.

Willoughby, H. E., D. P. Jorgensen, R. A. Black, and S. L. Rosenthal (1985), Project STORMFURY: A scientific chronicle 1962–1983, *Bull. Am. Meteorol. Soc.*, *66*, 505–514.

Yano, J.-I., and K. A. Emanuel (1991), An improved model of the equatorial troposphere and its coupling with the stratosphere, *J. Atmos. Sci.*, *48*, 377–389.

Zipser, E. J. (1977), Mesoscale and convective-scale downdrafts as distinct components of squall-line structure, *Mon. Weather Rev.*, *105*, 1568–1589.

————————————

M. T. Montgomery, Department of Meteorology, Naval Postgraduate School, 589 Dyer Rd. Monterey, CA 93943, USA.

W. D. Terwey, Department of Earth Sciences, University of South Alabama, 307 University Blvd., N. LSCB 136 Mobile, AL 36688-0002, USA. (terwey@atmos.colostate.edu)